

Charge transfer at the α -RuCl₃/MnPc interface

Tom Klaproth ^{1,*}, Martin Knupfer ¹, Anna Isaeva,^{2,1} Maria Roslova,¹ Bernd Büchner,^{1,3} and Andreas Koitzsch^{1,†}

¹Leibniz Institute for Solid State and Materials Research, PF 27 01 16, D-01171 Dresden, Germany

²Van der Waals-Zeeman Institute, Department of Physics and Astronomy, University of Amsterdam, Science Park 094, NL-1098 XH Amsterdam, The Netherlands

³Institut für Festkörperphysik, Technische Universität Dresden, D-01171 Dresden, Germany



(Received 2 August 2022; accepted 5 October 2022; published 17 October 2022)

The interface of manganese(II) phthalocyanine (MnPc) with an α -RuCl₃ single crystal is studied by means of photoelectron spectroscopy. The organic molecule was evaporated on top of an *in situ* cleaved α -RuCl₃ bulk crystal in steps. The work function and electron affinity of α -RuCl₃ is determined to be 6.3 and 5.4 eV, respectively, in line with common fluorinated acceptor molecules, but with the potential to absorb more electrons per area at interfaces with other materials. These favorable electronic properties lead to a charge transfer from MnPc to α -RuCl₃ which manifests itself mainly in peak shape changes of core level photoemission spectra and further filling of Ru 4*d* states as revealed by valence band photoemission. This work demonstrates the promising potential of α -RuCl₃ as a strong acceptor material for interfaces in general, and for organic molecules in particular.

DOI: [10.1103/PhysRevB.106.165418](https://doi.org/10.1103/PhysRevB.106.165418)

I. INTRODUCTION

The main focus of research concerning α -RuCl₃ lies on its exotic magnetic properties: The proximity to a Kitaev quantum spin liquid (QSL) state [1]. A prerequisite for Kitaev's model are spins $S = 1/2$ on a honeycomb lattice, which is realized in α -RuCl₃ due to its complex electronic structure: Ru³⁺ possesses a 4*d*⁵ configuration and a combination of octahedral crystal field splitting, spin-orbit coupling, and Mott physics leads to effective pseudospins 1/2 [2–4]. Various experimental techniques have been applied to determine the magnetic ground state, such as magnetization measurements, specific heat measurements, and neutron scattering, which turned out to be Heisenberg-type antiferromagnetic below 7 K [5]. Subsequently, the influence of external pressure and magnetic fields has been studied showing strong indications for a field-induced QSL state for fields above about 10 T [6–10]. Efforts to stabilize the QSL state in α -RuCl₃ are still pursued to this day.

Another less prominent property of α -RuCl₃ is its high work function, reported to be 6.1 eV [11] and found to be 6.3 eV in this work. This makes charge transfer processes at interfaces with other materials highly likely, e.g., the interface of graphene with α -RuCl₃, resulting in highly hole-doped graphene, is studied both theoretically and experimentally [12–16].

On the other hand, electronic devices made out of polymers and organic molecules are on the rise with organic LED (OLED) screens in a wide range of commercial products and more exotic devices being the subject of research in both

academia and industry [17,18]. Interfaces of two-dimensional (2D) inorganic with organic compounds are rarely studied, even though both research fields aim towards cost effective and high performance devices [19] and combining 2D materials such as WSe₂ with organic acceptor molecules leads to *p*-type doping at the interface [20]. The family of metal phthalocyanines (MPcs) features favorable electronic and optical properties as well as chemical stability and therefore has been considered for many technological applications such as molecular photovoltaics [21]. The electronic properties of MPcs also depend on the substrate underneath and can therefore be tuned [22]. If the central ion is a transition metal such as Fe, Mn, or Co, it carries an effective spin and applications in spintronics are possible [23,24]. In the case of manganese(II) phthalocyanine (MnPc), the central ion carries a spin $S = 3/2$ and a MnPc crystal shows ferromagnetic interactions [25,26]. Recently, the magnetic coupling of MnPc through interfaces was reported and shown to be tunable by electron doping, further pushing the field towards applications [27,28].

The present paper investigates the interface of an α -RuCl₃ bulk crystal with MnPc by means of ultraviolet (UPS) and x-ray photoelectron spectroscopy (XPS).

II. METHODS

The photoemission studies have been carried out using a two-chamber ultrahigh vacuum system (base pressure about 5×10^{-10} mbar). All core level data have been determined with a monochromized Al *K* α x-ray source (XR-50-M x-ray tube with Focus-500 monochromator) at room temperature. Ultraviolet photoelectron spectroscopy (UPS) was carried out using a helium gas discharge lamp UVS-300. The total energy resolution of the spectrometer equipped with a SPECS PHOIBOS-150 hemispherical analyzer was 0.15 eV for UPS

*t.klaproth@ifw-dresden.de

†a.koitzsch@ifw-dresden.de

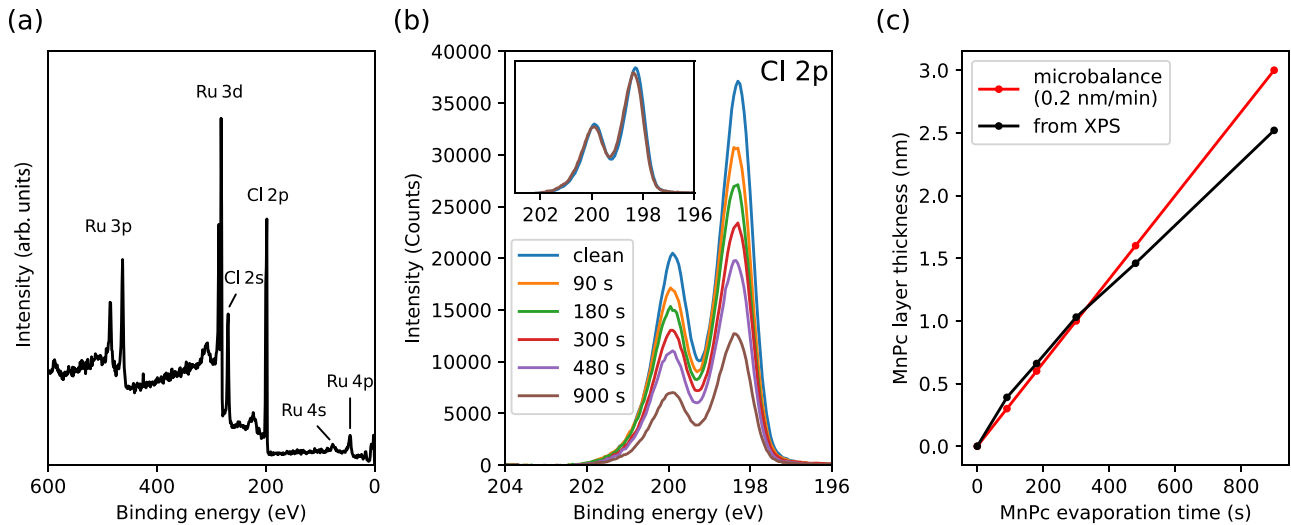


FIG. 1. (a) XPS survey of the clean α - RuCl_3 surface. Peaks are labeled based on their spectroscopic origin. (b) Cl $2p$ core level spectra for clean α - RuCl_3 and after each evaporation step. The signal attenuation can be used to quantitatively estimate the MnPc overlayer. Inset: Normalized Cl $2p$ spectra of the clean crystal and after 900 s of MnPc evaporation. (c) Evaluated layer thickness with respect to evaporation time and the prediction from the quartz crystal microbalance. The obtained thickness values from XPS will be used for all following figures.

and 0.35 eV for XPS. Valence band spectra were corrected for contributions of He $I\beta$ and He $I\gamma$ to the He $I\alpha$ main line at 21.21 eV assuming they had the same shape, intensities of 4.2% (He $I\beta$) and 1.1% (He $I\gamma$), and their energy being shifted towards lower binding energies by 1.87 eV (He $I\beta$) and 2.52 eV (He $I\gamma$). To obtain the secondary electron cutoff a bias voltage of 5 V is applied between the sample and analyzer. The photoelectrons were collected in normal emission with either UV or x-ray radiation impinging the sample at about 45° from the sample normal.

Plateletlike single crystals up to several mm in diameter of RuCl_3 were grown by chemical vapor transport reactions in the temperature gradient between 650 and 700 $^\circ\text{C}$ for 3–7 days. Their chemical composition and crystal structure were characterized by energy-dispersive x-ray spectroscopy and x-ray diffraction.

Manganese(II) phthalocyanine (MnPc) was obtained from a commercial source (Alfa Aesar) and purified by heating at 380 $^\circ\text{C}$ for approximately 3 days under UHV conditions.

The α - RuCl_3 crystal was cleaved under UHV conditions using Scotch tape. After initial spectroscopic measurements of the clean crystal, MnPc was deposited on top of the sample in steps by *in situ* thermal evaporation at around 435 $^\circ\text{C}$. The film thickness was controlled using a quartz crystal microbalance during the evaporation process and afterwards verified by the intensity reduction of the Ru Cl $2p$ core level of α - RuCl_3 .

III. RESULTS

In Fig. 1(a) we show core level photoemission data as obtained for the freshly cleaved α - RuCl_3 single crystal. The main spectroscopic features are labeled according to their origin. Only features related to α - RuCl_3 are present, indicating a clean surface after cleaving. This is supported especially by the absence of oxygen and carbon related XPS lines. Figure 1(b) presents the evolution of the Cl $2p$ core level upon stepwise evaporation of MnPc with the evaporation time

given in the legend. A Shirley background [29] was subtracted to set the background level to zero. The line shape remains unchanged as demonstrated in the inset of Fig. 1(b) comparing the spectra obtained for the clean crystal and after 900 s of MnPc evaporation normalized to the same peak area. The drop in intensity is due to the overlayer of MnPc attenuating the photoemission signal from the α - RuCl_3 crystal. This can be used to quantitatively estimate the MnPc layer thickness by assuming exponential dampening of the peak area and using the empirical electron mean free path formula for organic compounds found by Seah and Dench [30]. The entire peak area from 196 to 203 eV of the background subtracted spectra was integrated.

The evaluated layer thicknesses with respect to evaporation time is presented in Fig. 1(c) (black curve). Before each evaporation step, the quartz crystal microbalance was used to adjust the deposition rate to 0.2 nm/min which corresponds to thickness values given by the red curve. The two complementary methods agree well, demonstrating the high controllability of the preparation method and indicating layer-by-layer growth which is assumed for XPS signal attenuation. The deviation at the final evaporation step could be due to increased disorder and reduced sticking coefficient. From now on, we will refer to the MnPc thickness obtained from the XPS estimation rather than the evaporation time rounded to one decimal place. Note that the MnPc coverage of 0.4 nm after the initial evaporation step corresponds to one closed layer of MnPc assuming layer-by-layer growth [31].

For now, we will shift our attention to the UPS results presented in Fig. 2 and pick up the discussion of the XPS results later. Figure 2(a) shows the valence band spectroscopy results obtained with He $I\alpha$ (21.21 eV) radiation. The pure α - RuCl_3 spectrum matches published results and shows no signs of degradation. The uppermost valence peak is located at 1.6 eV and has a mainly Ru $4d$ character with five electrons in the $4d$ shell for a Ru^{3+} configuration [4]. Exposure to air or deliberate tuning attempts such as sputtering or deposition

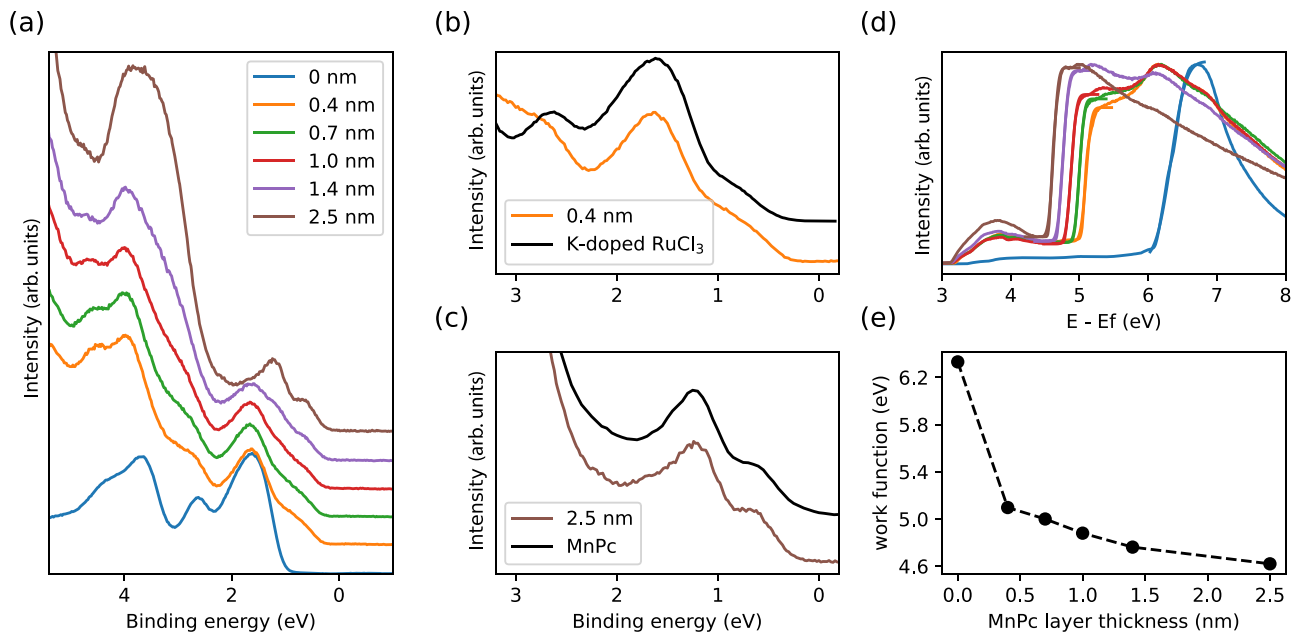


FIG. 2. (a) Valence band spectroscopy measured with He $I\alpha$ (21.21 eV) radiation depending on MnPc layer thickness. The curves are offset for clarity. (b) Comparison of the 0.4-nm MnPc spectrum with partially potassium-doped α -RuCl₃. (c) Comparison of the 2.5-nm MnPc spectrum with pure MnPc (10-nm MnPc on gold). (d) Secondary electron cutoff fitted with Heaviside functions to evaluate the work function. (e) Obtained work functions from the fitting procedure with respect to MnPc layer thickness.

of alkali metals onto the crystal surface lead to additional intensity at the lower binding energies due to further filling of the $4d$ shell [3,32,33]. No such signs are present in the spectrum of the freshly cleaved crystal. The spectrum at 2.5 nm MnPc coverage resembles that of pure MnPc as shown in Fig. 2(c) with the most prominent feature being the double peak structure of the uppermost valence band. The origin of the shoulder at lower energies is a singly occupied molecular orbital (SOMO) that is a hybrid state of Mn $3d$ and the ligand π orbitals (with a large Mn $3d$ contribution), whereas the main peak at 1.3 eV has a ligand π character only [34,35]. In the case of a charge transfer at an interface, the SOMO is emptied and the low-energy shoulder vanishes which should in principle be possible to observe in the spectra with intermediate coverage [36,37].

However, the shapes of spectra between the 0.4 and 1.0 nm MnPc overlayer are almost identical and only at 1.4 nm coverage, some additional intensity at around 1.3 eV is visible which corresponds to the position of the main peak of the MnPc highest occupied molecular orbital (HOMO). The reason is the dominant contribution of α -RuCl₃ to the overall UPS intensity, which can be explained by the following two arguments: First, the photoionization cross sections of Ru $4d$ and Cl $3p$, out of which the α -RuCl₃ valence band is comprised, are 4.2 and 2.3 times larger compared to C $2p$, respectively [38]. Second, the surface density of valence electrons is much higher in an α -RuCl₃ layer than in a MnPc layer. Using α -RuCl₃ crystal structure parameters found by Johnson *et al.* [5], the top layer unit cell covers $0.5976^2 \sin(60^\circ) \text{ nm}^2 \approx 0.3093 \text{ nm}^2$. On the other hand, a single flat-laying molecule covers an area of about $1.38 \times 1.38 \text{ nm}^2$ [39] [value for CuPc on highly oriented pyrolytic graphite (HOPG)], which is about 6.2 times the value of an α -RuCl₃ unit cell area. Integrating over the first 1 eV of the

occupied density of states of α -RuCl₃ (calculation taken from Ref. [3]) yields about 60 electrons per α -RuCl₃ layer within the area a MnPc molecule covers. The double peak valence structure of MnPc consists of three electrons in the case of no charge transfer, and two electrons if the SOMO is emptied at the interface per molecule. Therefore, the surface density of valence electrons in the region of interest should be about 20–30 times higher in α -RuCl₃ than in MnPc.

The most prominent change of the valence band between the clean α -RuCl₃ spectrum and the lowest coverage of 0.4 nm is the shoulder at lower binding energies. Figure 2(b) compares the 0.4 nm spectrum with that of a partially potassium-doped α -RuCl₃ crystal showing a very similar structure. The origin is additional filling of the Ru $4d$ level and a clear indication for a charge transfer towards α -RuCl₃ [32]. We can estimate the charge transferred towards α -RuCl₃ assuming one electron per MnPc molecule resulting in 0.081 electrons per ruthenium. The observed shoulder at a lower binding energy in Fig. 2(b) appears larger than the estimation suggests. Possible reasons could be a more dense stacking of the MnPc molecules than assumed, leading to a larger charge transfer, or modifications of the uppermost surface layer of RuCl₃ during the evaporation process, e.g., by the formation of a small amount of chlorine vacancies.

The secondary electron cutoff (SEC) is shown in Fig. 2(d) with Gaussian broadened Heaviside step functions fitted to determine the energy position [40,41]. All spectra show a small finite intensity at lower energies than the cutoff position due to the spot size of the lamp being slightly larger than the α -RuCl₃ crystal and some stray intensity being detected. The x-ray spot for the core level measurements is smaller, hence no such effects are seen in XPS measurements. The work function of pure α -RuCl₃ is 6.3 eV, in reasonable agreement with the literature [11]. The obtained values are presented

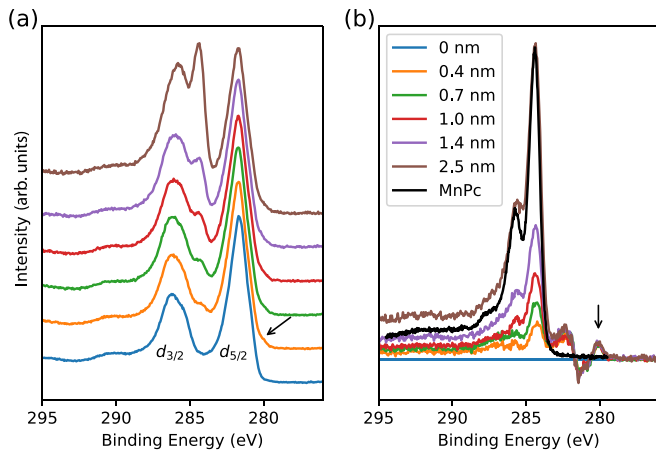


FIG. 3. (a) Ru $3d$ core level overlapping with the C $1s$ level measured with Al $K\alpha$ radiation depending on MnPc layer thickness. (b) The spectra shown in (a) with the clean α -RuCl $_3$ spectrum subtracted to reveal the C $1s$ shape and minor Ru $3d$ changes as well as a C $1s$ spectrum of pure MnPc (black).

in Fig. 2(e) and show a smooth evolution down to 4.6 eV for 2.5 nm MnPc coverage. The biggest change of 1.2 eV is observed between clean α -RuCl $_3$ and the thinnest coverage of 0.4 nm.

We will now discuss selected core levels that show signs of a charge transfer towards α -RuCl $_3$. The Ru $3d$ core level normalized to the $3d_{5/2}$ peak is shown in Fig. 3(a) with the C $1s$ level overlapping with the Ru $3d_{3/2}$ peak. Figure 3(b) presents the same spectra with the pure crystal being subtracted, hence the blue line in Fig. 3(b) corresponds to zero deviation. The subtracted spectra approximately correspond to C $1s$ originating from the MnPc cover and indeed show the double peak shape around 285 eV, as expected for MnPc [black curve in Fig. 3(b)]. At 280 eV binding energy, a weak shoulder to the $3d_{5/2}$ peak appears in the spectra with MnPc coverage indicated by arrows in Figs. 3(a) and 3(b). This feature does not stem from MnPc, as can be seen from the C $1s$ spectrum of pure MnPc in Fig. 3(b) showing no intensity near 280 eV. Rather, it is a small Ru $^{2+}$ contribution due to the charge transfer at the interface.

The effect on α -RuCl $_3$ core levels is small because of the low charge transfer towards α -RuCl $_3$ of about 0.081 electrons per ruthenium. Note that the XPS signal not only contains information about the top layer, but also a large contribution from the deeper layers in the bulk not effected by the charge transfer at the interface explaining the small effects seen in Fig. 3 compared to the larger effects in Fig. 2.

Therefore, core levels specifically related to MnPc are more suitable to study interface effects. For the lowest thickness of 0.4 nm almost all molecules will be in contact with α -RuCl $_3$, whereas at 2.5 nm coverage the signal will be dominated by molecules away from the interface. The Mn $2p_{3/2}$ core level spectra are shown in Fig. 4(a) with a linear background subtracted, a shift along the y axis to have equal intensity at 638 eV, as well as a slight smoothing applied for better comparison. The overall shape is controlled by an underlying multiplet structure [42,43] and changes with MnPc coverage as indicated by the left and right dashed lines mark-

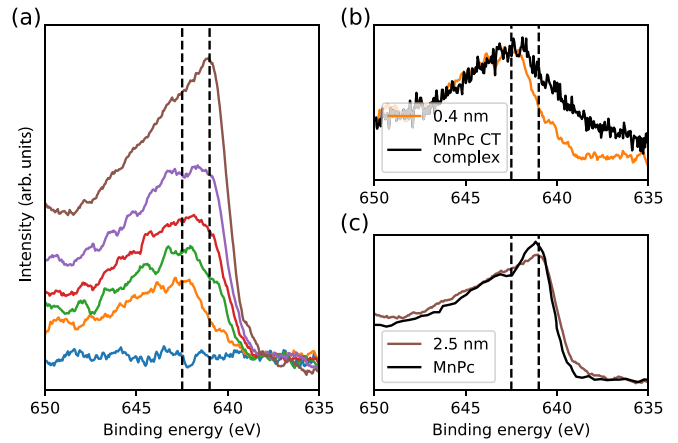


FIG. 4. (a) Mn $2p_{3/2}$ core level with the signal level on the right-hand side set to the same height, a linear background subtracted, and a slight smoothing applied. The main component for the 0.4- and 2.5-nm spectra marked by dashed lines proving the charge transfer. (b) Comparison of the 0.4-nm spectrum with the MnPc charge transfer complex (thin MnPc layer on F $_6$ TCNNQ). (c) Comparison of the 2.5-nm spectrum with bulk MnPc on gold (taken from Ref. [42]).

ing the energy position of the main peak component of the thinnest (642.5 eV) and thickest (641.0 eV) MnPc layer. The spectra for the lowest and highest MnPc coverage are compared to spectra of the charge transfer (CT) MnPc complex and pure MnPc in Figs. 4(b) and 4(c), respectively. The CT complex data were taken from an interface of F $_6$ TCNNQ with a 0.1 nm MnPc overlayer (see Ref. [37]). The 0.4 nm spectrum has an even lower intensity on the low-energy side compared to the CT complex, possibly indicating that Mn was not fully oxidized. However, the position of the maximum is nearly identical, confirming the charge transfer in our experiment. The Mn $2p_{3/2}$ spectra of the 2.5 nm layer agree reasonably well with the pure MnPc data [42]. Similar behavior of the Mn $2p_{3/2}$ spectra was observed for MnPc interfaces with various materials [36,37,44–47], with the higher-energy position being interpreted as an oxidation of the Mn central ion and therefore demonstrating the charge transfer from MnPc to α -RuCl $_3$ here as well.

Finally, Fig. 5 presents the energy scheme for α -RuCl $_3$ and MnPc with work function values for both materials, ionization potential IP for MnPc, as well as electron affinity E_{EA} and

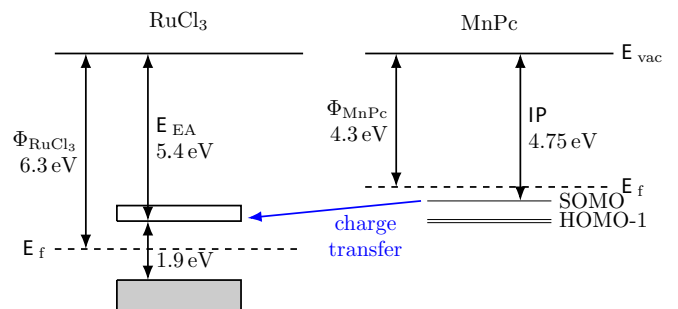


FIG. 5. Energy scheme of α -RuCl $_3$ and MnPc with work functions Φ given for both materials, ionization potential IP for MnPc, as well as electron affinity E_{EA} and band gap for α -RuCl $_3$.

band gap given for α -RuCl₃. Note that we took the work function and IP values for bulk MnPc from Ref. [48]. We estimate the electron affinity of α -RuCl₃ E_{EA} to be about 5.4 eV, favoring a charge transfer from the MnPc SOMO to α -RuCl₃. The value depends heavily on the assumed bare band gap. While gap values obtained from optical spectroscopy and electron energy-loss spectroscopy are affected by excitonic effects, we resort here to the value of $E_{\text{gap}}^{\text{bare}} = 1.9$ eV evaluated from the combination of photoemission and inverse photoemission by Sinn *et al.* [49].

IV. DISCUSSION AND SUMMARY

We expect α -RuCl₃ to be among the strongest acceptors available with an electron affinity E_{EA} of 5.4 eV, similar to various fluorinated organic molecules such as F₄TCNQ ($E_{EA} = 5.2$ eV) [50] or F₆TCNNQ ($E_{EA} = 5.0$ – 5.6 eV) [51,52]. However, α -RuCl₃ can absorb multiple electrons within the area such a molecule covers, most likely leading to an overall stronger doping effect as demonstrated with graphene [13,53].

As the amount of electrons transferred towards α -RuCl₃ is, in our case, mainly determined by the size of the molecule, choosing smaller or larger organic molecules could be an interesting approach for controlling doping levels at interfaces with inorganic compounds.

Changing the valence state of the transition metals due to charge transfers at interfaces changes the spin state of man-

ganese in MnPc and therefore its magnetic properties. The ground state of Mn in MnPc is reported as $(d_{xy})^1(d_{\pi})^3(d_{z^2})^1$ (the degenerate d_{zx} and d_{yz} are denoted as d_{π}) [54,55], with the states near the Fermi level being dominated by d_{zx} and d_{yz} orbitals [56]. Removing an electron due to the charge transfer may therefore lead to a higher spin state $S = 2$ and yield higher spin polarization near the Fermi level, advantageous for applications such as organic spin valves [24]. Applications in the field of single molecular magnets [57] enhancing the magnetic properties of a molecule on an α -RuCl₃ substrate may be possible as well.

In summary, we have studied the strong acceptorlike behavior of α -RuCl₃ by directly measuring its work function of 6.3 eV, estimating its electron affinity E_{EA} to be about 5.4 eV, and demonstrating a charge transfer at the interface with the organic semiconductor manganese(II) phthalocyanine (MnPc). The charge transfer is verified by the Mn $2p$ core level lying at higher binding energies for thin layers, slight changes in the Ru $3d$ line, and the valence band structure showing additional filling of the Ru $4d$ orbitals.

ACKNOWLEDGMENTS

We thank R. Hübel, F. Thunig, and M. Naumann for technical assistance. This work has been supported by the Deutsche Forschungsgemeinschaft (DFG) under the CRC “Correlated Magnetism—From Frustration to Topology” (SFB-1143, Project No. 247310070).

- [1] A. Kitaev, Anyons in an exactly solved model and beyond, *Ann. Phys.* **321**, 2 (2006).
- [2] K. W. Plumb, J. P. Clancy, L. J. Sandilands, V. V. Shankar, Y. F. Hu, K. S. Burch, H.-Y. Kee, and Y.-J. Kim, α -RuCl₃: A spin-orbit assisted Mott insulator on a honeycomb lattice, *Phys. Rev. B* **90**, 041112(R) (2014).
- [3] A. Koitzsch, C. Habenicht, E. Müller, M. Knupfer, B. Büchner, H. C. Kandpal, J. van den Brink, D. Nowak, A. Isaeva, and T. Doert, J_{eff} Description of the Honeycomb Mott Insulator α -RuCl₃, *Phys. Rev. Lett.* **117**, 126403 (2016).
- [4] L. J. Sandilands, Y. Tian, A. A. Reijnders, H.-S. Kim, K. W. Plumb, Y.-J. Kim, H.-Y. Kee, and K. S. Burch, Spin-orbit excitations and electronic structure of the putative Kitaev magnet α -RuCl₃, *Phys. Rev. B* **93**, 075144 (2016).
- [5] R. D. Johnson, S. C. Williams, A. A. Haghighirad, J. Singleton, V. Zapf, P. Manuel, I. I. Mazin, Y. Li, H. O. Jeschke, R. Valentí, and R. Coldea, Monoclinic crystal structure of α -RuCl₃ and the zigzag antiferromagnetic ground state, *Phys. Rev. B* **92**, 235119 (2015).
- [6] R. Yadav, N. A. Bogdanov, V. M. Katukuri, S. Nishimoto, J. van den Brink, and L. Hozoi, Kitaev exchange and field-induced quantum spin-liquid states in honeycomb α -RuCl₃, *Sci. Rep.* **6**, 37925 (2016).
- [7] Z. Wang, S. Reschke, D. Hüvonen, S.-H. Do, K.-Y. Choi, M. Gensch, U. Nagel, T. Rößm, and A. Loidl, Magnetic Excitations and Continuum of a Possibly Field-Induced Quantum Spin Liquid in α -RuCl₃, *Phys. Rev. Lett.* **119**, 227202 (2017).
- [8] Y.-F. Jiang, T. P. Devereaux, and H.-C. Jiang, Field-induced quantum spin liquid in the Kitaev-Heisenberg model and its relation to α -RuCl₃, *Phys. Rev. B* **100**, 165123 (2019).
- [9] G. Bastien, G. Garbarino, R. Yadav, F. J. Martinez-Casado, R. Beltran Rodriguez, Q. Stahl, M. Kusch, S. P. Limandri, R. Ray, P. Lampen-Kelley, D. G. Mandrus, S. E. Nagler, M. Roslova, A. Isaeva, T. Doert, L. Hozoi, A. U. B. Wolter, B. Buchner, J. Geck, and J. van den Brink, Pressure-induced dimerization and valence bond crystal formation in the Kitaev-Heisenberg magnet α -RuCl₃, *Phys. Rev. B* **97**, 241108(R) (2018).
- [10] Y. Cui, J. Zheng, K. Ran, J. Wen, Z.-X. Liu, B. Liu, W. Guo, and W. Yu, High-pressure magnetization and NMR studies of α -RuCl₃, *Phys. Rev. B* **96**, 205147 (2017).
- [11] I. Pollini, Electronic properties of the narrow-band material α -RuCl₃, *Phys. Rev. B* **53**, 12769 (1996).
- [12] S. Biswas, Y. Li, S. M. Winter, J. Knolle, and R. Valentí, Electronic Properties of α -RuCl₃ in Proximity to Graphene, *Phys. Rev. Lett.* **123**, 237201 (2019).
- [13] D. J. Rizzo, B. S. Jessen, Z. Sun, F. L. Ruta, J. Zhang, J.-Q. Yan, L. Xian, A. S. McLeod, M. E. Berkowitz, K. Watanabe *et al.*, Charge-transfer plasmon polaritons at graphene/ α -RuCl₃ interfaces, *Nano Lett.* **20**, 8438 (2020).
- [14] Y. Wang, J. Balgley, E. Gerber, M. Gray, N. Kumar, X. Lu, J.-Q. Yan, A. Fereidouni, R. Basnet, S. J. Yun *et al.*, Modulation doping via a two-dimensional atomic crystalline acceptor, *Nano Lett.* **20**, 8446 (2020).
- [15] J. Balgley, J. Butler, S. Biswas, Z. Ge, S. Lagasse, T. Taniguchi, K. Watanabe, M. Cothrine, D. G. Mandrus, J. Velasco, Jr. *et al.*, Ultrasharp lateral p-n junctions in modulation-doped graphene, *Nano Lett.* **22**, 4124 (2022).
- [16] D. J. Rizzo, S. Shabani, B. S. Jessen, J. Zhang, A. S. McLeod, C. Rubio-Verdú, F. L. Ruta, M. Cothrine, J. Yan, D. G. Mandrus

- et al.*, Nanometer-scale lateral p–n junctions in graphene/ α -RuCl₃ heterostructures, *Nano Lett.* **22**, 1946 (2022).
- [17] K. Walzer, B. Maennig, M. Pfeiffer, and K. Leo, Highly efficient organic devices based on electrically doped transport layers, *Chem. Rev.* **107**, 1233 (2007).
- [18] X. Yang, A. Guo, L. Guo, Y. Liu, X. Sun, and Y. Guo, Organic semiconductors for room-temperature spin valves, *ACS Mater. Lett.* **4**, 805 (2022).
- [19] C. V. S. Batista, L. Mercas, C. A. R. Costa, D. H. S. de Camargo, and C. C. B. Bufon, High-performance ultrathin molecular rectifying diodes based on organic/inorganic interface engineering, *Adv. Funct. Mater.* **32**, 2108478 (2022).
- [20] F. R ckerl, T. Klaproth, R. Schuster, B. B chner, and M. Knupfer, Surface functionalization of WSe₂ by F₁₆CoPc, *Phys. Status Solidi B* **254**, 1600656 (2017).
- [21] G. Bottari, G. de la Torre, D. M. Guldi, and T. Torres, Covalent and noncovalent phthalocyanine-carbon nanostructure systems: Synthesis, photoinduced electron transfer, and application to molecular photovoltaics, *Chem. Rev.* **110**, 6768 (2010).
- [22] S. Mandal, M. Mukherjee, and S. Hazra, Evolution of electronic structures of polar phthalocyanine–substrate interfaces, *ACS Appl. Mater. Interfaces* **12**, 45564 (2020).
- [23] J. Tong, L. Ruan, X. Yao, G. Qin, and X. Zhang, Defect states dependence of spin transport in iron phthalocyanine spin valves, *Phys. Rev. B* **99**, 054406 (2019).
- [24] A. Banerjee, B. Kundu, and A. J. Pal, Introducing immobilized metal phthalocyanines as spin-injection and detection layers in organic spin-valves: Spin-tunneling and spin-transport regimes, *Org. Electron.* **41**, 173 (2017).
- [25] C. Barraclough, R. Martin, S. Mitra, and R. Sherwood, Paramagnetic anisotropy, electronic structure, and ferromagnetism in spin $S = 3/2$ manganese (II) phthalocyanine, *J. Chem. Phys.* **53**, 1638 (1970).
- [26] Y. Taguchi, T. Miyake, S. Margadonna, K. Kato, K. Prassides, and Y. Iwasa, Synthesis, structure, and magnetic properties of Li-doped manganese-phthalocyanine, Li_x[MnPc] ($0 \leq x \leq 4$), *J. Am. Chem. Soc.* **128**, 3313 (2006).
- [27] G. Avvisati, P. Gargiani, P. Mondelli, F. Presel, A. Baraldi, and M. G. Betti, Superexchange pathways stabilize the magnetic coupling of MnPc with Co in a spin interface mediated by graphene, *Phys. Rev. B* **98**, 115412 (2018).
- [28] G. Avvisati, P. Gargiani, C. Mariani, and M. G. Betti, Tuning the magnetic coupling of a molecular spin interface via electron doping, *Nano Lett.* **21**, 666 (2021).
- [29] D. A. Shirley, High-resolution x-ray photoemission spectrum of the valence bands of gold, *Phys. Rev. B* **5**, 4709 (1972).
- [30] M. P. Seah and W. Dench, Quantitative electron spectroscopy of surfaces: A standard data base for electron inelastic mean free paths in solids, *Surf. Interface Anal.* **1**, 2 (1979).
- [31] H. Yamada, T. Shimada, and A. Koma, Preparation and magnetic properties of manganese (II) phthalocyanine thin films, *J. Chem. Phys.* **108**, 10256 (1998).
- [32] A. Koitzsch, C. Habenicht, E. Muller, M. Knupfer, B. Buchner, S. Kretschmer, M. Richter, J. van den Brink, F. Boerrnert, D. Nowak, A. Isaeva, and T. Doert, Nearest-neighbor Kitaev exchange blocked by charge order in electron-doped α -RuCl₃, *Phys. Rev. Mater.* **1**, 052001(R) (2017).
- [33] X. Zhou, H. Li, J. A. Waugh, S. Parham, H.-S. Kim, J. A. Sears, A. Gomes, H.-Y. Kee, Y.-J. Kim, and D. S. Dessau, Angle-resolved photoemission study of the Kitaev candidate α -RuCl₃, *Phys. Rev. B* **94**, 161106(R) (2016).
- [34] M. Grobosch, B. Mahns, C. Loose, R. Friedrich, C. Schmidt, J. Kortus, and M. Knupfer, Identification of the electronic states of manganese phthalocyanine close to the Fermi level, *Chem. Phys. Lett.* **505**, 122 (2011).
- [35] N. Marom and L. Kronik, Density functional theory of transition metal phthalocyanines, II: Electronic structure of MnPc and FePc-symmetry and symmetry breaking, *Appl. Phys. A* **95**, 165 (2009).
- [36] F. R ckerl, B. Mahns, E. Dodbiba, V. Nikolis, M. Herzig, B. B chner, M. Knupfer, T. Hahn, and J. Kortus, Electronic properties of the charge transfer material MnPc/F₄TCNQ, *J. Chem. Phys.* **145**, 114702 (2016).
- [37] D. Waas, F. R ckerl, and M. Knupfer, Charge transfer at the interface between MnPC and F₆TCNNQ, *Phys. Status Solidi B* **256**, 1800245 (2019).
- [38] J. Yeh and I. Lindau, Atomic subshell photoionization cross sections and asymmetry parameters: $1 \leq Z \leq 103$, *At. Data Nucl. Data Tables* **32**, 1 (1985).
- [39] S. Wang, X. Dong, C. Lee, and S. Lee, Ordered growth of copper phthalocyanine on highly oriented pyrolytic graphite (HOPG) at high substrate temperatures, *J. Phys. Chem. B* **108**, 1529 (2004).
- [40] T. Schultz, T. Lenz, N. Kotadiya, G. Heimel, G. Glasser, R. Berger, P. W. Blom, P. Amsalem, D. M. de Leeuw, and N. Koch, Reliable work function determination of multicomponent surfaces and interfaces: The role of electrostatic potentials in ultraviolet photoelectron spectroscopy, *Adv. Mater. Interfaces* **4**, 1700324 (2017).
- [41] O. Renault, R. Brochier, A. Roule, P.-H. Haumesser, B. Kr mker, and D. Funnemann, Work-function imaging of oriented copper grains by photoemission, *Surf. Interface Anal.* **38**, 375 (2006).
- [42] T. Kroll, R. Kraus, R. Sch nfelder, V. Y. Aristov, O. Molodtsova, P. Hoffmann, and M. Knupfer, Transition metal phthalocyanines: Insight into the electronic structure from soft x-ray spectroscopy, *J. Chem. Phys.* **137**, 054306 (2012).
- [43] H. Nesbitt and D. Banerjee, Interpretation of XPS Mn(2p) spectra of Mn oxyhydroxides and constraints on the mechanism of MnO₂ precipitation, *Am. Mineral.* **83**, 305 (1998).
- [44] S. Lindner, M. Knupfer, R. Friedrich, T. Hahn, and J. Kortus, Hybrid States and Charge Transfer at a Phthalocyanine Heterojunction: MnPc^{δ+}/F₁₆CoPc^{δ-}, *Phys. Rev. Lett.* **109**, 027601 (2012).
- [45] F. R ckerl, D. Waas, B. B chner, M. Knupfer, D. R. Zahn, F. Haidu, T. Hahn, and J. Kortus, Charge transfer from and to manganese phthalocyanine: Bulk materials and interfaces, *Beilstein J. Nanotechnol.* **8**, 1601 (2017).
- [46] S. Lindner, B. Mahns, A. K nig, F. Roth, M. Knupfer, R. Friedrich, T. Hahn, and J. Kortus, Phthalocyanine dimers in a blend: Spectroscopic and theoretical studies of MnPc^{δ+}/F₁₆CoPc^{δ-}, *J. Chem. Phys.* **138**, 024707 (2013).
- [47] J. L. Zhang, Z. Wang, J. Q. Zhong, K. D. Yuan, Q. Shen, L. L. Xu, T. C. Niu, C. D. Gu, C. A. Wright, A. Tadich *et al.*, Single-molecule imaging of activated nitrogen adsorption on individual manganese phthalocyanine, *Nano Lett.* **15**, 3181 (2015).
- [48] F. Haidu, A. Fechner, G. Salvan, O. Gordan, M. Fronk, D. Lehmann, B. Mahns, M. Knupfer, and D. Zahn, Influence of film thickness and air exposure on the transport gap of manganese phthalocyanine, *AIP Adv.* **3**, 062124 (2013).

- [49] S. Sinn, C. H. Kim, B. H. Kim, K. D. Lee, C. J. Won, J. S. Oh, M. Han, Y. J. Chang, N. Hur, H. Sato *et al.*, Electronic structure of the Kitaev material α -RuCl₃ probed by photoemission and inverse photoemission spectroscopies, *Sci. Rep.* **6**, 39544 (2016).
- [50] W. Gao and A. Kahn, Controlled *p* doping of the hole-transport molecular material *N,N'*-diphenyl-*N,N'*-bis(1-naphthyl)-1,1'-biphenyl-4,4'-diamine with tetrafluorotetracyanoquinodimethane, *J. Appl. Phys.* **94**, 359 (2003).
- [51] M. L. Tietze, L. Burtone, M. Riede, B. Lüssem, and K. Leo, Fermi level shift and doping efficiency in *p*-doped small molecule organic semiconductors: A photoelectron spectroscopy and theoretical study, *Phys. Rev. B* **86**, 035320 (2012).
- [52] H. Méndez, G. Heimel, A. Opitz, K. Sauer, P. Barkowski, M. Oehzelt, J. Soeda, T. Okamoto, J. Takeya, J.-B. Arlin *et al.*, Doping of organic semiconductors: Impact of dopant strength and electronic coupling, *Angew. Chem.* **125**, 7905 (2013).
- [53] C. Coletti, C. Riedl, D. S. Lee, B. Krauss, L. Patthey, K. von Klitzing, J. H. Smet, and U. Starke, Charge neutrality and band-gap tuning of epitaxial graphene on SiC by molecular doping, *Phys. Rev. B* **81**, 235401 (2010).
- [54] F. Petraki, H. Peisert, P. Hoffmann, J. Uihlein, M. Knupfer, and T. Chassé, Modification of the 3d-electronic configuration of manganese phthalocyanine at the interface to gold, *J. Phys. Chem. C* **116**, 5121 (2012).
- [55] M.-S. Liao, J. D. Watts, and M.-J. Huang, DFT study of unligated and ligated manganese porphyrins and phthalocyanines, *Inorg. Chem.* **44**, 1941 (2005).
- [56] T. Q. Nguyen, M. C. S. Escano, and H. Kasai, Nitric oxide adsorption effects on metal phthalocyanines, *J. Phys. Chem. B* **114**, 10017 (2010).
- [57] L. Bogani and W. Wernsdorfer, Molecular spintronics using single-molecule magnets, in *Nanoscience and Technology: A Collection of Reviews from Nature Journals* (World Scientific, Singapore, 2010), pp. 194–201.